substance: Ti_2O_3
property: properties of doped Ti_2O_3

Ti_2O_3:V: Addition of small amounts of V appears to mimic the temperature increase. Studies of lattice parameters: [74R, 76C, 77R2, 77R3], axial and equatorial interatomic distances: Fig. 1. Lattice properties show marked changes [75B, 74S]. Raman spectrum shows the softening of the lowest A_{1g} und E_g modes (Fig. 2) to follow closely the behaviour of the pure material on heating (Fig. 3). The temperature variation of the A_{1g} and E_g modes is essentially suppressed for $x > 0.12$ in $(Ti_{1-x}V_x)_2O_3$ (Fig. 4). The heat capacity anomaly (see below) at ca. 470 K is also suppressed for $x > 0.04$ [73B].

The heat capacity of V-doped Ti_2O_3 shows a marked anomaly at low temperature [73S2, 79M]. Initially this was interpreted in terms of a one dimensional conductivity model [72S]; but this idea was shown to be untenable [73Z1, 73Z2], and an electronic model invoking a very narrow V a_1 band was proposed. Subsequent magnetic measurements [75D1, 75D2, 75E, 77D, 78D, 79D1] have established that, for $x < 0.02$, localized magnetic moments exist on V, but decrease with increasing x. Above $x = 0.007$ a spin-glass forms at very low temperature, and it is this transition from spin-glass to a paramagnetic metal with no magnetic moment on the V that gives rise to the heat capacity anomaly [79D1].

Conductivity in Ti_2O_3:V: Fig. 5. The transition onset temperature remains constant up to the point where it disappears, and the apparent activation energy falls smoothly from 0.0254 eV in pure Ti_2O_3 to zero at 2.6 at % V [70C]. Similar Seebeck data: Fig. 6. Phase diagram: Fig. 7 and [80D].

Ti_2O_3:Sc: Structural changes reported in [77R1], electrical properties in [74C]. ρ first decreases with x and then increases. Seebeck coefficient shows much reduced phonon effect at low temperatures, perhaps because impurity scattering dominates.

References:

70C Chandrashekhar, G. V., Won Choi, Q., Moyo, J., Honig, J. M.: Mater. Res. Bull. 5 (1970) 999.
72S Sjostrand, M. E., Keesom, P. H.: Phys. Lett. A39 (1972) 147.
73B Barros, H. L., Chandrashekhar, G. V., Chi, T. C., Honig, J. M., Sladek, R. J.: Phys. Rev. B7 (1973) 5147.
73S1 Shin, S. H., Chandrashekhar, G. V., Loehman, R. E., Honig, J. M.: Phys. Rev. B8 (1973) 1364.
73S2 Sjostrand, M. E., Keesom, P. H.: Phys. Rev. B7 (1973) 3558.
73Z1 van Zandt, L. L., Eklund, P. C.: Phys. Rev. B7 (1973) 1454.
73Z2 van Zandt, L. L.: Phys. Rev. Lett. 31 (1973) 598.
74C Chandrashekhar, G. V., van Zandt, L. L., Honig, J. M., Jayaraman, A.: Phys. Rev. B10 (1974) 5063.
74R Robinson, W. R.: J. Solid State Chem. 9 (1974) 255.
74S Shin, S. H., Aggarwal, R. L., Lax, B., Honig, J. M.: Phys. Rev. B9 (1974) 583.
75B Bennett, J. G., Sladek, R. J.: J. Solid State Chem. 12 (1975) 370.
75D1 Dumas, J., Schlenker, C., Natoli, P. C.: Solid State Commun. 16 (1975) 493.
75D2 Dumas, J., Schlenker, C., Tholence, J. L., Tournier, R.: Solid State Commun. 17 (1975) 1215.
75E Eagen, C. F., Koon, N. C., van Zandt, L. L.: AIP Conf. Proc. 29 (1975) 590.
76C Caponi, J. J., Marezio, M., Dumas, J., Schlenker, C.: Solid State Commun. 20 (1976) 893.
77D Dumas, J., Schienker, C., Tholence, J. L., Tournier, R.: Physica 86-88b (1977) 867.
77R1 Rice, C. E., Robinson, W. R.: J. Solid State Chem. 21 (1977) 155.
77R2 Rice, C. E., Robinson, W. R.: Mater. Res. Bull. 12 (1977) 421.
77R3 Rice, C. E., Robinson, W. R.: J. Solid State Chem. 21 (1977) 145.
78D Dumas, J., Schlenker, C.: J. Mag. Magn. Mater. 7 (1978) 252.
79D1 Dumas, J., Schlenker, C., Tholence, J. L., Tournier, R.: Phys. Rev. B20 (1979) 3913.
79D2 Dumas, J., Schlenker, C.: J. Phys. C12 (1979) 2381.
79M Miyako, Y., Sato, T., Kimishima, Y., Yuochumas, Y. G.: J. Phys. Soc. Jpn. 46 (1979) 1379.
80D Dumas, J.: Phys. Rev. B22 (1980) 5085.

Fig. 1.

$(Ti_{1-x}M_x)_2O_3$, M = V, Sc, Al. Interatomic distances vs. composition parameter x [77R2].

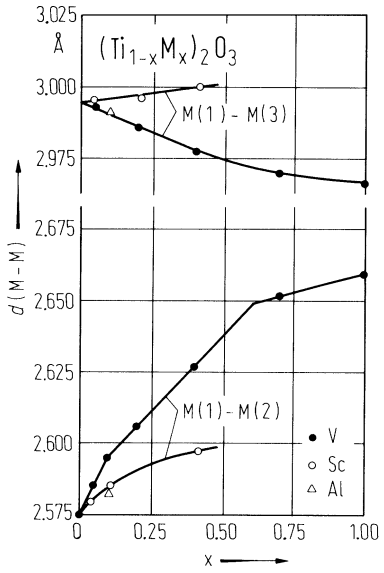

Fig. 2.

$(Ti_{1-x}V_x)_2O_3$. Phonon wavenumbers vs. composition parameter x at 300 K [74S].

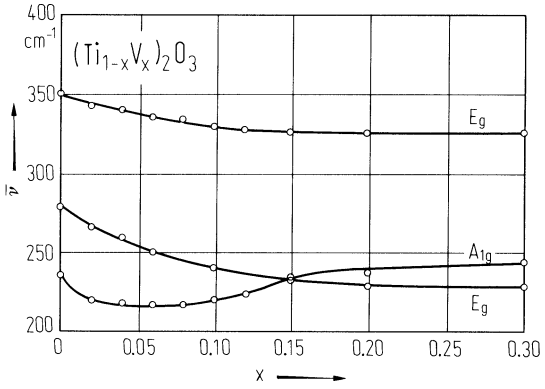

Fig. 3.

Ti_2O_3. Wavenumbers of Raman frequencies vs. temperature [74S].

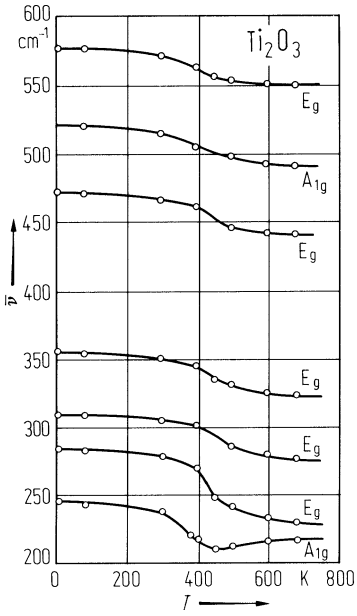

Fig. 4.

$(Ti_{1-x}V_x)_2O_3$. Wavenumbers of the A_{1g}-mode vs. temperature for samples of different compositions [74S].

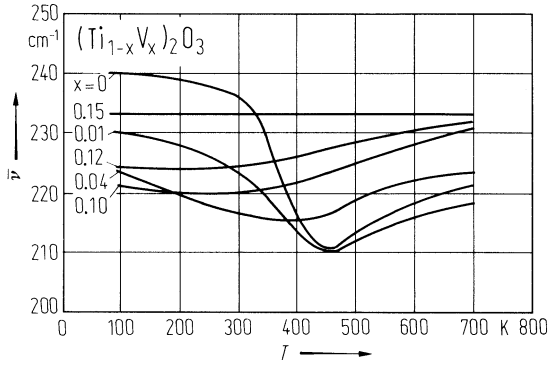

Fig. 5.

$(Ti_{1-x}V_x)_2O_3$. Resistivity vs. reciprocal temperature for polycrystalline samples of different compositions [70C]. Dashed line: transition temperature from semiconductor to metal.

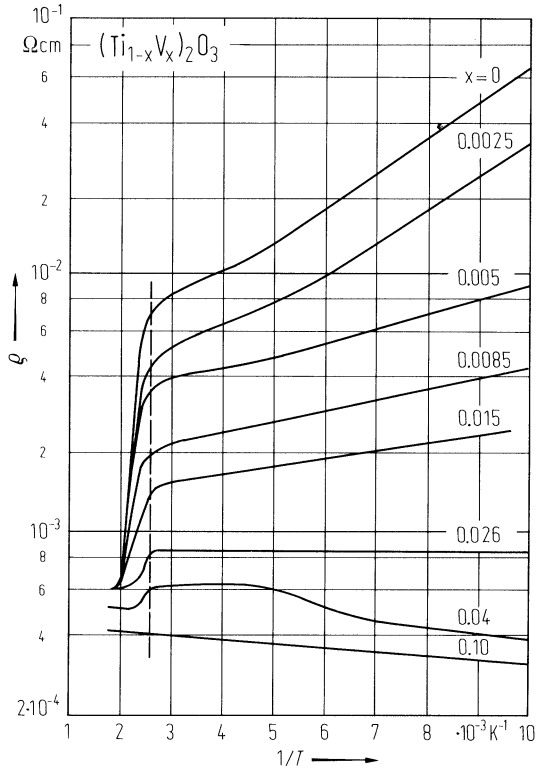

Fig. 6.

$(Ti_{1-x}V_x)_2O_3$. Seebeck coefficient vs. temperature for polycrystalline doped samples of different compositions and for single crystals of Ti_2O_3 [73S1].

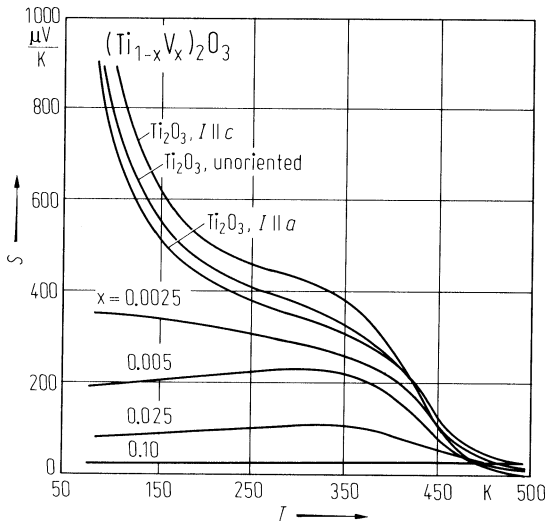

Fig. 7.

$(Ti_{1-x}V_x)_2O_3$. Phase diagram. A: spin glass, B: mictomagnetic, C: antiferromagnetic metal, D: antiferromagnetic semiconductor, E: paramagnetic semiconductor, F: paramagnetic metal [79D2].